ISSN 0021-3640, JETP Letters, 2017, Vol. 106, No. 5, pp. 302–307. © Pleiades Publishing, Inc., 2017.
Original Russian Text © V.V. Val'kov, A.D. Fedoseev, 2017, published in Pis'ma v Zhurnal Eksperimental'noi i Teoreticheskoi Fiziki, 2017, Vol. 106, No. 5, pp. 282–287.

CONDENSED MATTER

Fano Antiresonance Induced by the Rashba Spin–Orbit Coupling in Systems with Conduction Channels Exhibiting the Points of Nonanalyticity in Fermion Paths

V. V. Val'kov* and A. D. Fedoseev

Kirensky Institute of Physics, Federal Research Center KSC, Siberian Branch, Russian Academy of Sciences, Krasnoyarsk, 660036 Russia

**e-mail: vvv@iph.krasn.ru*

Received July 25, 2017

It is shown that the combined effect of the nonanalyticity of the channel for the motion of charge carriers and the Rashba spin–orbit coupling induces resonant anomalies in the transport characteristics of nanosystems related to the size quantization. When the characteristic length determined by the ratio of the hopping integral and the spin–orbit coupling constant coincides with the distance between the points of nonanalyticity, the size effect arises in the channel. It manifests itself in the complete reflection from the device, which can be treated as the Fano antiresonance. The current–voltage characteristics of the nanosystem with the nonanalytical channel undergo significant changes at slight variations of the spin–orbit coupling constant near its critical value.

DOI: 10.1134/S0021364017170131

1. INTRODUCTION

The low-dimensional systems with spin–orbit coupling are of special current interest related to the studies of the characteristics of topological insulators [1–4]. The edge states in such systems are characterized by the tight correlation between the direction of motion of an electron and its spin direction. As a result, the motion of a fermion can occur without its scattering by nonmagnetic impurities.

In the studies of effects of the Rashba field on the properties of low-dimensional systems [5], the possible existence of points corresponding to the nonanalyticity of the paths and thus to the stepwise changes in the Rashba field is usually ignored. In addition, the characteristics of the edge states are studied using the models infinite in one direction [6, 7]. The problem of the possibility of applying the results of such analysis to finite systems having the points of nonanalyticity in the charge carrier paths is rather topical. In this connection, the authors of [8] pointed to the importance of study of a square system. However, a detailed analysis of the effect of corners has not been undertaken yet.

Earlier, the authors of [9] reported that the Rashba spin–orbit coupling could break symmetry in topological insulators. In such a case, the quasiparticle states cannot be classified according to the spin projection and the effect of broken symmetry manifests itself in the change in quasiparticle spin direction in the course of its motion. However, the existence of corners was disregarded in [9] and the spin oscillation was assumed to depend on the crystal momentum.

The importance of the inhomogeneity of the Rashba spin–orbit coupling for low-dimensional systems was demonstrated in [10], where the effect of the inhomogeneity of the spin–orbit coupling constant on the spin transport in two-dimensional systems was shown. However, the problem concerning the directional inhomogeneity of the Rashba field was not considered.

Neglecting the existence of corners in the system can be a good approximation if the electron mean free path is much smaller than the length of the side in the system under study. However, in low-dimensional systems, such approach could be rather inadequate. For this reason, this work is aimed at the analysis of the effect of nonanalyticity in the charge carrier paths on the quantum transport.

2. DEVICE ON A SUBSTRATE EXHIBITING THE POINTS OF NONANALYTICITY IN THE CHARGE-TRANSFER CHANNEL

To study the combined effect of the Rashba spin–orbit coupling and the nonanalyticity of the fermion paths in a one-dimensional channel, we discuss the transport characteristics of the one-dimensional chain of sites located on the sides of a square (Fig. 1). The sites of such a system, which we for brevity refer to

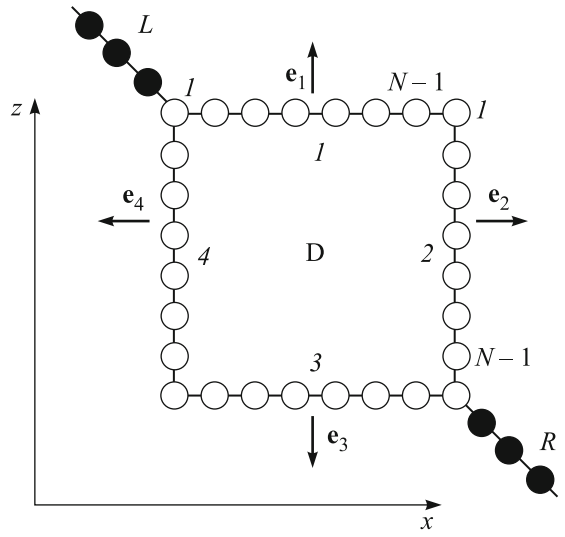

Fig. 1. Layout of the system and the numeration of the sites for the nonanalytical chain with the point contacts symmetrically connected to it.

below as the nonanalytical chain (NC), are denoted as open circles. Each rectilinear segment contains N sites and the total number of sites in the NC equals $4(N-1)$.

To simplify the inclusion of the Rashba spin–orbit coupling in the NC, we represent the Hamiltonian in the form

$$\hat{\mathcal{H}}_{\rm D} = -t_{\rm D}\sum_{nj\sigma} a^{+}_{jn+1\sigma}a_{jn\sigma} - t_{\rm D}\sum_{j\sigma} a^{+}_{j+1,1\sigma}a_{j,N-1\sigma}$$
$$- {\rm i}\alpha_{\rm D}\sum_{nj\sigma\sigma'} (\mathbf{e}_j\boldsymbol{\tau}_{\sigma'\sigma}) a^{+}_{jn+1\sigma'}a_{jn\sigma} \qquad (1)$$
$$- {\rm i}\alpha_{\rm D}\sum_{j\sigma\sigma'} (\mathbf{e}_j\boldsymbol{\tau}_{\sigma'\sigma}) a^{+}_{j,1\sigma'}a_{j+1,N-1\sigma} + {\rm H.c.}$$

Here, the first two terms describe the hoppings between the nearest neighbors characterized by the parameter $t_{\rm D} > 0$, whereas the next two terms correspond to the Rashba spin–orbit coupling related to the gradient of the electrical potential in the direction perpendicular to plane of the square. The subscript $j = 1, 2, 3, 4$ enumerates the sides of the square in the clockwise direction, $n = 1, \ldots, N-1$ enumerates the sites on each side, $\alpha_{\rm D}$ is the Rashba spin–orbit coupling constant, $\sigma = \pm 1$ denotes the electron spin projection on the quantization axis z, $\mathbf{e}_j$ is the unit vector along the direction of the Rashba field (see Fig. 1), and $\boldsymbol{\tau}$ are the Pauli matrices. It is important that the direction of the Rashba field is individual for each side of the square: it lies in the plane of the square and is perpendicular to the corresponding side.

The one-electron eigenstates of Hamiltonian (1) can be represented in the form

$$\psi = \sum_{j=1}^{4}\sum_{n=1}^{N-1}\sum_{\sigma} z_{jn\sigma}a^{+}_{jn\sigma}|0\rangle, \qquad (2)$$

where $|0\rangle$ is the vacuum state. Taking into account the symmetry axis C_4 passing through the center of the square perpendicular to the plane of the NC allows us to write the one-electron states as [11]

$$E_{mls} = -2\sqrt{t_{\rm D}^2 + \alpha_{\rm D}^2}\cos k_{mls}, \qquad (3)$$
$$k_{mls} = \frac{1}{N-1}\left[s\arccos\left(\frac{\cos\chi}{\sqrt{2}}\right) + \phi_l + 2\pi m\right],$$
$$l = -2, -1, 0, 1, \quad s = \pm 1, \quad m = 1, \ldots, (N-1),$$
$$\chi = k_0(N-1), \quad \phi_l = \frac{\pi}{2}l + \frac{\pi}{4},$$
$$z^{mls}_{1n\uparrow} = \frac{1}{2\sqrt{N-1}}\frac{1}{\sqrt{1+\rho_s^2}}e^{{\rm i}k_0(n-n_c)-{\rm i}s\pi/4}e^{-{\rm i}kn},$$
$$z^{mls}_{1n\downarrow} = \frac{1}{2\sqrt{N-1}}\frac{\rho_s}{\sqrt{1+\rho_s^2}}e^{-{\rm i}k_0(n-n_c)+{\rm i}s\pi/4}e^{-{\rm i}kn},$$
$$\rho_s = \sqrt{1+\sin^2\chi} - s\sin\chi,$$
$$z^{mls}_{1+j,n\sigma} = e^{-{\rm i}\phi_l j}\left[z^{mls}_{1n\sigma}\cos(\pi j/4) - \sigma z^{mls}_{1n\overline{\sigma}}\sin(\pi j/4)\right],$$

where k_0 is inverse to the characteristic spin–orbit coupling length $L_{\rm so}$ (the distance at which the electron spin rotates about the Rashba field direction by an angle of π). In the tight-binding approximation, k_0 is determined by the expression

$$k_0 = \arcsin\left(\alpha_{\rm D}/\sqrt{t_{\rm D}^2 + \alpha_{\rm D}^2}\right). \qquad (4)$$

The length scale $L_{\rm so}$ gives rise to the parameter χ of NC, which is determined by the ratio of the length of the side of the square $L = N-1$ (in units of interatomic distance) and the length $L_{\rm so}$:

$$\chi = \frac{\pi}{2}\frac{L}{L_{\rm so}}. \qquad (5)$$

3. LANDAUER–BÜTTIKER FORMALISM FOR THE NONANALYTICAL CHAIN WITH CONTACTS

In the study of the electric current flowing through the nonanalytical chain, we assume that the chain is connected to contacts, which can be treated as macroscopic conductors. The electrons involved in the reservoir are thermalized and have the temperature and chemical potential of a contact before their returning to the device. Thus, an electron incident on the contact should be completely absorbed by it and thermalized before its return to the device.

To find the coefficient of transmission through the device, we should solve the Schrödinger equation with the Hamiltonian [12]

$$\hat{H} = \hat{H}_{\rm L} + \hat{T}_{\rm L} + \hat{H}_{\rm D} + \hat{T}_{\rm R} + \hat{H}_{\rm R}, \tag{6}$$

$$\hat{H}_{\rm L} = \sum_{n=-\infty,\sigma}^{-1} \left[t_{\rm L}(c^{+}_{n-1\sigma}c_{n\sigma} + c^{+}_{n\sigma}c_{n-1\sigma}) - \varepsilon_d c^{+}_{n\sigma}c_{n\sigma} \right],$$

$$\hat{H}_{\rm R} = \sum_{n=1,\sigma}^{\infty} \left[t_{\rm R}(c^{+}_{n+1\sigma}c_{n\sigma} + c^{+}_{n\sigma}c_{n+1\sigma}) - \varepsilon_d c^{+}_{n\sigma}c_{n\sigma} \right],$$

$$\hat{T}_{\rm L} = t_{\rm LD}\sum_{\sigma}\left(c^{+}_{-1\sigma}a_{\rm L\sigma} + a^{+}_{\rm L\sigma}c_{-1\sigma} \right),$$

$$\hat{T}_{\rm R} = t_{\rm RD}\sum_{\sigma}\left(c^{+}_{1\sigma}a_{\rm R\sigma} + a^{+}_{\rm R\sigma}c_{1\sigma} \right),$$

$$\hat{H}_{\rm D} = \sum_{mls} E_{mls} b^{+}_{mls} b_{mls}.$$

Here, $\hat{H}_{\rm L,R}$ are the Hamiltonians describing electrons in the left (L) and right (R) contacts, operators $\hat{T}_{\rm L,R}$ take into account the existence of the tunnel coupling between the contacts and device, $a_{\rm L,R}$ is the annihilation operator for an electron at a site in the device directly connected to the corresponding contact, and b_{mls} is the annihilation operator for a one-electron excitation (3) in the device. We assume that the one-site energy in the device is shifted with respect to that in the contacts by ε_d and the energy E of the incident electron is measured from the one-site energy in the device.

The transport characteristics of the NC are determined from the calculation of the wavefunction of the system in the electron scattering problem. We write the wavefunction as an expansion in the complete basis of the system

$$\Psi = \sum_{n=-\infty,\sigma}^{-1} u_{n\sigma}c^{+}_{n\sigma}|0\rangle + \sum_{mls} w_{mls}b^{+}_{mls}|0\rangle + \sum_{n=1,\sigma}^{\infty} v_{n\sigma}c^{+}_{n\sigma}|0\rangle. \tag{7}$$

The coefficients of the expansion for the left contact correspond to the superposition of the incident and reflected waves

$$u_{n\sigma} = p_\sigma e^{{\rm i}k_{\rm L}n} + r_\sigma e^{-{\rm i}k_{\rm L}n}, \quad |p_\uparrow|^2 + |p_\downarrow|^2 = 1,$$

whereas only the transmitted component is taken into account for the right contact:

$$v_{n\sigma} = t_\sigma e^{{\rm i}k_{\rm R}n}.$$

The parameter p_σ determines the polarization of an incident electron, and the wave vectors $k_{\rm L,R}$ are measured in units of the inverse interatomic distance.

The parameters of the expansion satisfy the following set of inhomogeneous differential equations:

$$E = 2t_{\rm L}\cos k_{\rm L} - \varepsilon_d, \quad E = 2t_{\rm R}\cos k_{\rm R} - \varepsilon_d,$$
$$-t_{\rm L}r_\sigma + \sum_{mls} t_{\rm LD}w_{mls}z^{mls}_{L\sigma} = t_{\rm L}p_\sigma,$$
$$-t_{\rm R}t_\sigma + \sum_{mls} t_{\rm RD}w_{mls}z^{mls}_{R\sigma} = 0, \tag{8}$$
$$(E_{mls} - E)w_{mls} + \sum_{\sigma}\left(t_{\rm LD}r_\sigma e^{{\rm i}k_{\rm L}} z^{mls*}_{\rm L\sigma} + t_{\rm RD}t_\sigma e^{ik_{\rm R}} z^{mls*}_{R\sigma} \right) = -t_{\rm LD}\sum_{\sigma} p_\sigma e^{-ik_{\rm L}} z^{mls*}_{\rm L\sigma}.$$

The coefficients of reflection and transmission are determined in terms of the ratio of the reflected and transmitted probability flow, respectively, and the incident flow

$$R = \sum_{\sigma}|r_\sigma|^2, \quad T = \frac{t_{\rm R}\sin k_{\rm R}}{t_{\rm L}\sin k_{\rm L}}\sum_{\sigma}|t_\sigma|^2. \tag{9}$$

4. FANO ANTIRESONANCES IN THE TRANSPORT CHARACTERISTIC OF A NONANALYTICAL CHAIN

A typical form of the transmission coefficients for the NC with the contacts connected symmetrically with respect to the square center (see Fig. 1) is illustrated in Fig. 2. This figure demonstrates that the Rashba spin–orbit coupling leads to the destructive interference of the wavefunctions corresponding to the charge carrier motion along the two channels, giving rise to the Fano antiresonances. The number of such antiresonances is determined by the number of energy eigenvalues of the chain, which are fourfold degenerate in the absence of the spin–orbit coupling, and is equal to $(2(N-1)-1)$.

To understand the mechanism underlying the Fano antiresonances, we consider the behavior of the excitations corresponding to the eigenstates in the device as a function of the parameter $0 \le \chi \le \pi/2$ given by Eq. (5). For symmetrically connected contacts, it is important to know the relation between the coefficients in the expansion for wavefunctions of one-electron states in the chain (3) at the sites connected to the contacts

$$z^{mls}_{\rm R\sigma} = {\rm i}(-1)^l \sigma z^{mls}_{\rm L\bar{\sigma}}, \tag{10}$$

which is determined by the parity of orbital quantum number l and is independent of m and s.

At $\alpha_{\rm D} = 0$, all one-electron states are fourfold degenerate except for the edge ones corresponding to

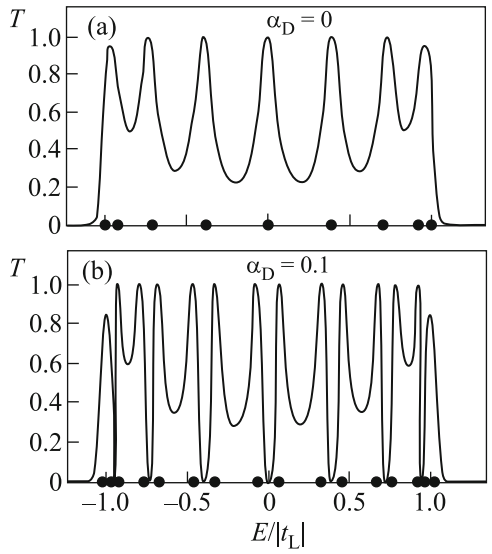

Fig. 2. Transmission coefficient for the nonanalytical chain with the parameters $t_L = t_R = -1$, $t_D = 0.5$, $\varepsilon_D = 0$, $t_{LD} = t_{RD} = -0.5$, and $N = 5$ and with the spin–orbit coupling constant α_D = (a) 0 and (b) 0.1. Closed circles denote the eigenenergies of one-particle states in the nonanalytical chain.

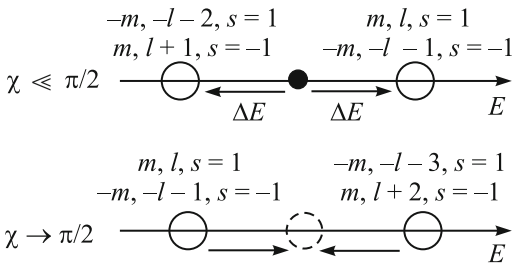

Fig. 3. Variation of the eigenenergies of one-particle excitations at $\alpha_D \ll t_D$ and at α_D close to the critical value.

the top and bottom of the band, which are doubly degenerate with respect to $s = \pm 1$. Each fourfold degenerate energy corresponds to the following sets of the quantum numbers:

$$\begin{aligned} &\text{(i) } m, l, s = 1, \quad \text{(ii) } (-m), (-l-2), s = 1, \\ &\text{(iii) } m, (l+1), s = -1, \quad \text{(iv)} (-m), (-l-1), s = -1. \end{aligned} \tag{11}$$

It is implied that, for l coming outside the enumeration limits mentioned in (3), it is necessary to make the replacements $l \to l \pm 4$ and $m \to m \mp 1$. Such replacement does not affect the parity of the orbital quantum number.

At $\alpha_D \neq 0$, the fourfold degeneracy is lifted and all energies become doubly degenerate. Note that, for any (mls) state, there exists such $(m'l', s' = s)$ state for which $E_{m'l's'} = -E_{mls}$ and the parity of the orbital quantum number is the same for both of these states, $(-1)^l = (-1)^{l'}$. Let us write Eqs. (8) for such pairs of states:

$$\begin{aligned} &-t_L r_\sigma + \sum_{mls}{}' t_{LD}(w_{mls} + w_{m'l's'}) z_{L\sigma}^{mls} = t_L p_\sigma, \\ &-t_R t_\sigma + \sum_{mls}{}' t_{RD}(w_{mls} + w_{m'l's'}) z_{R\sigma}^{mls} = 0, \\ &(E_{mls} - E) w_{mls} + \sum_\sigma \Big(t_{LD} r_\sigma e^{ik_L} z_{L\sigma}^{mls*} \\ &+ t_{RD} t_\sigma e^{ik_R} z_{R\sigma}^{mls*} \Big) = -t_{LD} \sum_\sigma p_\sigma e^{-ik_L} z_{L\sigma}^{mls*}, \\ &(-E_{mls} - E) w_{m'l's'} + \sum_\sigma \Big(t_{LD} r_\sigma e^{ik_L} z_{L\sigma}^{mls*} \\ &+ t_{RD} t_\sigma e^{ik_R} z_{R\sigma}^{mls*} \Big) = -t_{LD} \sum_\sigma p_\sigma e^{-ik_L} z_{L\sigma}^{mls*}. \end{aligned} \tag{12}$$

Here, the sums with prime denote the summation over the aforementioned pairs of states. In such case, it is easy to show that $w_{mls} = -w_{m'l's'}$ and $t_\sigma = 0$ at $E = 0$, which gives rise to the Fano antiresonance.

The degeneracy is lifted by the spin–orbit coupling in such a way that the energies of the states with the same quantum number s and the parity of the orbital quantum number l are shifted in the opposite directions (Fig. 3). Then, at small α_D values, one should expect an antiresonance within the range between each pair of doubly degenerate energies because the main contribution to series expansion (7) comes just from these pairs of states and all above reasons are still valid. The numerical calculations show that this antiresonance appears at any α_D value (see Fig. 2).

5. COMPLETE REFLECTION EFFECT INDUCED BY THE RASHBA SPIN–ORBIT COUPLING

In the case of $\chi \sim \pi/2$, corresponding to the situation where the characteristic length of the Rashba spin–orbit coupling is close to the length of the side of the square, the transmission coefficient vanishes for the whole energy range except for the vicinities of the energies corresponding to the one-electron excited eigenstates E_{mls} in the NC (Fig. 4). Such an effect means the existence of a nearly isolated device with weak coupling to the contacts.

For the interpretation of this effect, we analyze the eigenstates of the device at $\chi = \pi/2$. In the case under study, all one-electron eigenenergies of the NC turn out to be fourfold degenerate. It is important that the states with m, l, s and $m' = -m$, $l' = -l - 1 - 2s$, $s' = s$

(see Fig. 3), for which the orbital quantum numbers have different parities, have the same energy. For such pairs of coefficients, Eqs. (8) can be rewritten using Eq. (10) in the form

$$(E_{mls} - E)(w_{m'l's'} - w_{mls}) = 2t_{\mathrm{RD}}e^{ik_{\mathrm{R}}}\sum_{\sigma} t_{\sigma}z_{\mathrm{R}\sigma}^{mls*},$$

$$-t_{\mathrm{R}}t_{\sigma} + \sum_{mls}{}' t_{\mathrm{RD}}(w_{mls} - w_{m'l's'})z_{\mathrm{R}\sigma}^{mls} = 0.$$

The analysis of these equations shows that the transmission coefficient T vanishes at any $E \neq E_{mls}$.

At $\chi \approx \pi/2$, at energies far from the eigenenergies E_{mls}, the above argumentation is still valid. Hence, we should expect that the transmission coefficient T will be nonzero only within a certain range near the excitation eigenenergies of the chain. This conclusion is indeed supported by the numerical calculations (see Fig. 4).

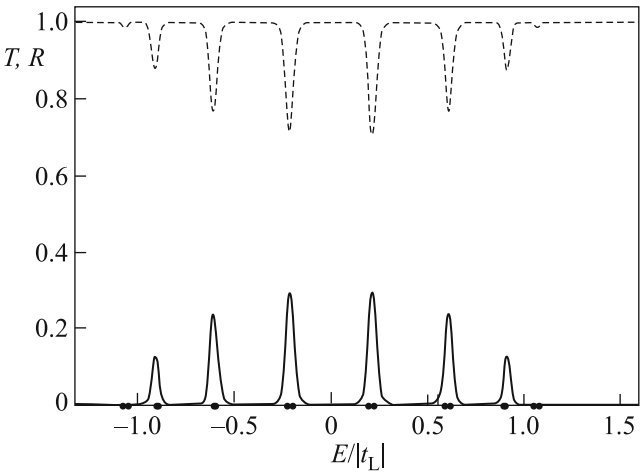

Fig. 4. Coefficients of (solid line) transmission and (dashed line) reflection for the case of $\chi \approx \pi/2$. $t_{\mathrm{L}} = t_{\mathrm{R}} = -1$, $t_{\mathrm{D}} = 0.5$, $\alpha_{\mathrm{D}} = 0.2$, $\varepsilon_d = 0$, $t_{\mathrm{LD}} = t_{\mathrm{RD}} = -0.5$, and $N = 5$. Closed circles denote the eigenenergies of one-particle states in the nonanalytical chain.

6. CURRENT–VOLTAGE CHARACTERISTICS FOR THE NONANALYTICAL CHAIN

In the Landauer–Büttiker representation, the electric current flowing across the device connected to one-dimensional contacts is given by the expression

$$I = I_{\mathrm{LR}} - I_{\mathrm{RL}},$$

$$I_{\mathrm{LR}} = \frac{2e}{L}\sum_{k}\frac{1}{\hbar}\left(\frac{\partial E}{\partial k}\right)T_{\mathrm{LR}}(E)f_{\mathrm{L}}(E), \qquad (13)$$

$$I_{\mathrm{RL}} = \frac{2e}{L}\sum_{k}\frac{1}{\hbar}\left(\frac{\partial E}{\partial k}\right)T_{\mathrm{RL}}(E)f_{\mathrm{R}}(E).$$

Here, $f_{\mathrm{L,R}}(E) = f(E - \mu_{\mathrm{L,R}})$ is the Fermi distribution function for electrons and T_{LR} and T_{RL} are the transmission coefficients for an electron moving from the left contact to the right one and vice versa, respectively, which are calculated with the following additional term in Hamiltonian (6):

$$\hat{H}_V = \sum_{n=-\infty,\sigma}^{-1} eV_{\mathrm{L}}c_{n\sigma}^{+}c_{n\sigma} + \sum_{n=1,\sigma}^{\infty} eV_{\mathrm{R}}c_{n\sigma}^{+}c_{n\sigma}, \qquad (14)$$

describing the voltage applied across the contacts. The device itself is assumed to be grounded. Passing in Eq. (13) from summation over crystal momentum to integration with respect to energy, we find the final expression for the current flowing across the device (see, e.g., [13]):

$$I(V_{\mathrm{L}},V_{\mathrm{R}}) = \frac{2e}{h}\int dE\,[T_{\mathrm{LR}}f_{\mathrm{L}}(E) - T_{\mathrm{RL}}f_{\mathrm{R}}(E)]. \qquad (15)$$

Here, we take into account that the transmission coefficient for the system under study turns out to be independent of the spin direction of an incident electron.

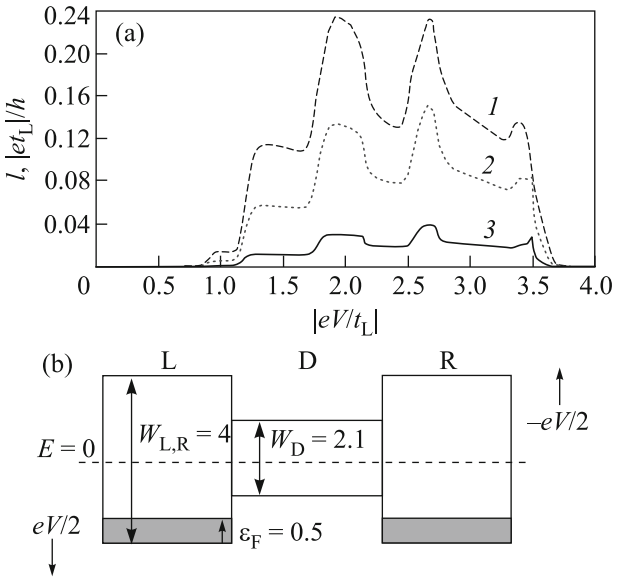

Fig. 5. (a) Current–voltage characteristic for the case of $\chi \approx \pi/2$. $t_{\mathrm{L}} = t_{\mathrm{R}} = -1$, $t_{\mathrm{D}} = 0.5$, $\varepsilon_d = 0$, $t_{\mathrm{LD}} = t_{\mathrm{RD}} = -0.5$, $N = 5$, $\varepsilon_{\mathrm{F}} = 0.5$, and $V_{\mathrm{L}} = -V_{\mathrm{R}} = V/2$. (*1*) $\alpha_{\mathrm{D}} = 0.18$; (*2*) $\alpha_{\mathrm{D}} = 0.19$; (*3*) $\alpha_{\mathrm{D}} = 0.2$. (b) Energy diagram of the device and contacts.

A typical form of the current–voltage characteristics for the NC is illustrated in Fig. 5. The size of the steps is determined by the Rashba spin–orbit coupling up to the complete locking of the electric current by the system. In turn, the Rashba spin–orbit coupling can be controlled by the applied electric field (as was

shown in [14]). This allows using the suggested system as a basic circuit in microelectronic devices.

All results presented in Figs. 2–5 were obtained for a square with a small ($N = 5$) side length and with an admittedly large value of the spin–orbit coupling constant α_D only for a better visualization of the effects under study. For the actual systems, the characteristic length of the Rashba spin–orbit coupling is about 90–300 nm [15, 16]. Thus, to satisfy the $\chi \approx \pi/2$ condition, we should use a square including hundreds of sites. However, all results obtained above are still valid while the electron transport across the system remains ballistic. If the number of sites in the system is large, the numerical technique developed in [17] turns out to be quite efficient, whereas for the analytical treatment, it is more convenient to use Eqs. (8).

7. CONCLUSIONS

The essential result of our study is the prediction of the size-effect Fano antiresonance resulting from the combined effect of the Rashba spin–orbit coupling and the nonanalyticity of the charge carrier paths in the one-dimensional fermion chain at a substrate. The Fano antiresonance appears each time when the characteristic length determined by the ratio of the hopping parameter and the Rashba spin–orbit coupling constant multiplied by some odd number becomes equal to the distance between the given points of nonanalyticity.

The study of this effect has been performed using the calculations of the transport characteristics for the one-dimensional fermion chain with the sequence of sites corresponding to their location on the sides of a square. In the tight-binding approximation, we have calculated the transmission coefficient and the current–voltage characteristic of such system using the Landauer–Büttiker method. It has been shown that, at the symmetric connection to the contacts, the interference of the wavefunctions for electrons propagating along two channels gives rise to the aforementioned Fano antiresonances. It is important that, at the value of the spin–orbit coupling parameter close to the critical one when the characteristic length corresponding to the Rashba spin–orbit coupling approaches the length of the side of the square, the complete reflection of an electron from the system occurs at all energies except for those corresponding to the one-electron excitations in the nonanalytical chain. Near this critical point, the variation of the spin–orbit coupling by the applied electric field strongly affects the current–voltage characteristic, which makes it possible to use the nonanalytical chain in the circuitry of microelectronic devices.

This work was funded by the Russian Foundation for Basic Research (project nos. 16-42-242036, 16-42-243056, and 17-42-240441), Government of the Krasnoyarsk Territory, Krasnoyarsk Region Science and Technology Support Fund to the Research (project nos. 21/16, 29/16, and 02/17).

REFERENCES

1. X.-L. Qi, Rev. Mod. Phys. **83**, 1057 (2011).
2. D. V. Khomitsky and A. A. Chubanov, J. Exp. Theor. Phys. **118**, 457 (2014).
3. M. Ezawa, Phys. Rev. Lett. **114**, 056403 (2015).
4. V. A. Volkov and V. E. Enaldiev, J. Exp. Theor. Phys. **122**, 608 (2016).
5. Yu. A. Bychkov and E. I. Rashba, JETP Lett. **39**, 78 (1984).
6. C. L. Kane and E. J. Mele, Phys. Rev. Lett. **95**, 226801 (2005).
7. L. I. Magarill and M. V. Entin, JETP Lett. **100**, 561 (2014).
8. M. Lee, H. Khim, and M.-S. Choi, Phys. Rev. B **89**, 035309 (2014).
9. A. Rod, T. L. Schmidt, and S. Rachel, Phys. Rev. B **91**, 245112 (2015).
10. G. Seibold, S. Caprara, M. Grilli, and R. Raimondi, J. Magn. Magn. Mater. **440**, 63 (2017).
11. V. V. Val'kov and A. D. Fedoseev, J. Magn. Magn. Mater. **440**, 185 (2016).
12. V. V. Val'kov and S. V. Aksenov, J. Exp. Theor. Phys. **113**, 266 (2011).
13. S. Datta, *Electronic Transport in Mesoscopic Systems* (Cambridge Univ. Press, Cambridge, 1995).
14. J. Nitta, T. Akazaki, and H. Takayanagi, Phys. Rev. Lett. **78**, 1335 (1997).
15. C. Flindt, A. S. Sorensen, and K. Flensberg, Phys. Rev. Lett. **97**, 240501 (2006).
16. S. Nadj-Perge, V. S. Pribiag, J. W. G. van den Berg, K. Zuo, S. R. Plissard, E. P. A. M. Bakkers, S. M. Frolov, and L. P. Kouwenhoven, Phys. Rev. Lett. **108**, 166801 (2012).
17. A. F. Sadreev and I. Rotter, J. Phys. A: Math. Gen. **36**, 11413 (2003).

Translated by K. Kugel